JACS
JOURNAL OF THE AMERICAN CHEMICAL SOCIETY
pubs.acs.org/JACS
Article

Installing Controlled Stereo-Defects Yields Semicrystalline and Biodegradable Poly(3-Hydroxybutyrate) with High Toughness and Optical Clarity

Ethan C. Quinn, Andrea H. Westlie, Ainara Sangroniz, Maria Rosaria Caputo, Shu Xu, Zhen Zhang, Meltem Urgun-Demirtas, Alejandro J. Müller,* and Eugene Y.-X. Chen*

Cite This: J. Am. Chem. Soc. 2023, 145, 5795−5802
Read Online
ACCESS | Metrics & More | Article Recommendations | Supporting Information

ABSTRACT: Stereo-defects present in stereo-regular polymers often diminish thermal and mechanical properties, and hence suppressing or eliminating them is a major aspirational goal for achieving polymers with optimal or enhanced properties. Here, we accomplish the opposite by introducing controlled stereo-defects to semicrystalline biodegradable poly(3-hydroxybutyrate) (P3HB), which offers an attractive biodegradable alternative to semicrystalline isotactic polypropylene but is brittle and opaque. We enhance the specific properties and mechanical performance of P3HB by drastically toughening it and also rendering it with the desired optical clarity while maintaining its biodegradability and crystallinity. This toughening strategy of stereo-microstructural engineering without changing the chemical compositions also departs from the conventional approach of toughening P3HB through copolymerization that increases chemical complexity, suppresses crystallization in the resulting copolymers, and is thus undesirable in the context of polymer recycling and performance. More specifically, syndio-rich P3HB (*sr*-P3HB), readily synthesized from the eight-membered *meso*-dimethyl diolide, has a unique set of stereo-microstructures comprising enriched syndiotactic [*rr*] and no isotactic [*mm*] triads but abundant stereo-defects randomly distributed along the chain. This *sr*-P3HB material is characterized by high toughness (U_T = 96 MJ/m^3) as a result of its high elongation at break (>400%) and tensile strength (34 MPa), crystallinity (T_m = 114 °C), optical clarity (due to its submicron spherulites), and good barrier properties, while it still biodegrades in freshwater and soil.

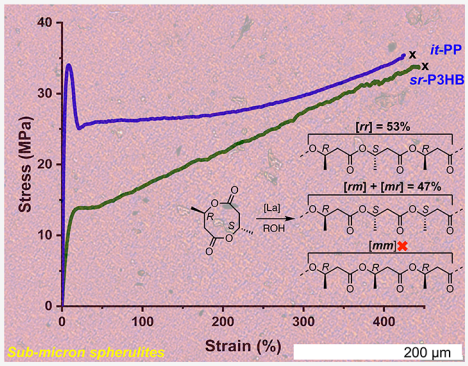

INTRODUCTION

Among several strategies[1−16] being developed to combat the current plastic problem,[17−21] biobased and biodegradable polymers[22−25] offer a more sustainable and environmentally benign alternative to the petroleum-based and nondegradable incumbent plastics. In particular, polyhydroxyalkanoates (PHAs), a class of biopolymers that can be synthesized biologically[26−34] and chemocatalytically,[35−38] are biodegradable in ambient environments, thus attracting intense interest. Purely isotactic poly(3-hydroxybutyrate) (*it*-P3HB), the most commonly produced PHA, exhibits several favorable properties including high crystallinity, melting transition temperature (T_m, 170−180 °C), and ultimate tensile strength (σ_B = ∼35 MPa), as well as excellent barrier properties. However, its perfect stereo-regularity and thus high crystallinity bring about its extreme brittleness, with elongation at break (ε_B) ∼ 3−6%, which largely limits its broader applications, especially in packaging.[39,40]

Biological routes produce isotactic (*R*)-polymers or copolymers of largely random sequences with dispersity (*Đ*) ≥2 due to the step-growth polymerization mechanism.[26,29−32,35] Chemical synthesis of PHA that operates on the catalyzed ring-opening polymerization (ROP) proceeds via a rapid chain-growth mechanism, which comes with the advantages of faster reaction kinetics and precision control over both PHA chain structures (predictable number-average molar mass (M_n) and low-to-near unity *Đ* values) and stereo-microstructures (tacticities).[36] For example, the ROP of *β*-butyrolactone (*β*-BL) produces diverse P3HB materials that are atactic (*at*),[41−50] iso-rich,[51−59] and syndiotactic (*st*) or syndio-rich (*sr*).[60−65] The ROP of racemic eight-membered dimethyl diolide (*rac*-8DL^{Me}) catalyzed by C_2-chrial salen-based metal complexes results in biomimetic *it*-P3HB.[66] This platform based on the diolides having two stereogenic centers was extended to afford stereo-sequenced stereo-block P3HB and other PHAs[67] including alternating isotactic PHAs,[68] both with enhanced ductility. Another method to toughen P3HB is through copolymerization of *rac*-8DL^{Me} with *rac*-8DL^{R} with

Received: December 4, 2022
Published: March 3, 2023

https://doi.org/10.1021/jacs.2c12897
J. Am. Chem. Soc. 2023, 145, 5795−5802

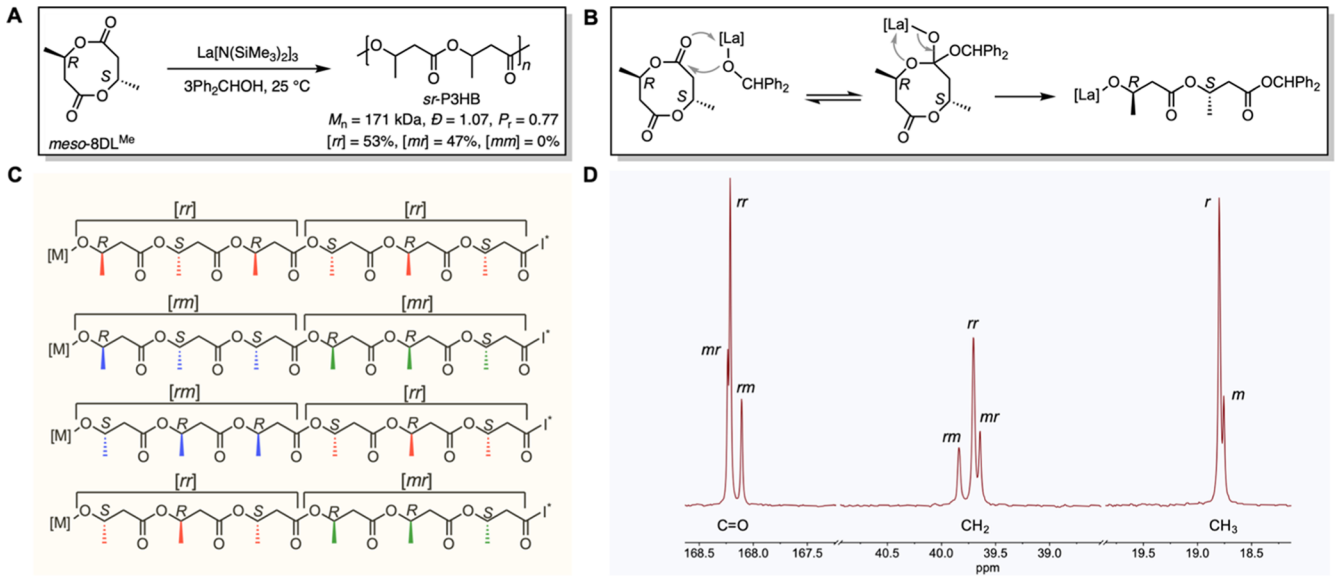

Figure 1. (A) Overall reaction scheme for the synthesis of *sr*-P3HB. (B) Highlighted key steps of monomer coordination, migratory insertion, and ring opening proposed in the coordination-insertion ROP of *meso*-8DL^{Me} using the La catalyst. (C) Listed all possible stereo-chemical outcomes from the metal-catalyzed ROP of *meso*-8DL^{Me} toward *sr*-P3HB, specifically showing the impossibility of generating [*mm*] triads (in the absence of other side reactions). (D) Semiquantitative ^{13}C NMR spectrum ($CDCl_3$, 23 °C) of *sr*-P3HB (M_n = 171 kDa, $Đ$ = 1.07) in the carbonyl, methylene, and methyl regions.

Table 1. Selected Results of the ROP of *meso*-8DL^{Me} Catalyzed by [La] with Different Alcohol Initiators[a]

run	[M]/[La]/[ROH]	[ROH]	time (min)	conv. (%)[c]	M_n[d] (kDa)	$Đ$[d] (M_w/M_n)	[*rr*][e] (%)	[*mr*][e] (%)	P_r[e]
1	5000:1:3	$PhCH_2OH$	45	75	77.3	1.05	54	46	0.77
2	5000:1:3	Ph_2CHOH	3	78	146	1.09	53	47	0.77
3	5000:1:3	Ph_3COH	1,230	8	35.6	1.02	n.d	n.d	n.d
4	5000:1:3[b]	Ph_2CHOH	22	89	171	1.07	53	47	0.77

[a]Conditions: precatalyst [La] = La[$N(SiMe_3)_2$]$_3$, monomer (M) = *meso*-8DL^{Me} = 100 mg (0.58 mmol) in dichloromethane (0.3 mL), 1.94 M, ~25 °C, except for run 4. [b]Conditions for run 4: [La], *meso*-8DL^{Me} = 1.2 g (7.0 mmol) in dichloromethane (4.6 mL), 1.50 M, ~25 °C. [c]Monomer conversion determined by ^{1}H NMR analysis. [d]Absolute weight-average molecular weight (M_w), number-average molecular weight (M_n), and dispersity ($Đ = M_w/M_n$) determined by size exclusion chromatography (SEC) coupled with a Wyatt DAWN HELEOS II multi (18)angle light scattering detector and a Wyatt Optilab TrEX dRI detector and performed at 40 °C in chloroform. [e]Calculated from semiquantitative^{13}C NMR spectrum (CDCl3, 23 °C; Figures S8−10). n.d. = not determined due to low conversion of this run.

longer alkyl pendant groups (R = Et, ^{n}Bu), which created tough, polyolefin-like thermoplastics.[67,69] The copolymerization of *rac*-8DL^{Me} has been extended to other lactones, yielding toughened P3HB.[70,71]

Although the copolymerization strategy employed in the biological and chemical routes effectively toughens P3HB, increasing the chemical complexity and suppressing the crystallization in the form of copolymers are undesirable in the context of polymer recycling and performance. Considering the emerging needs for the monomaterial product design and the fact that tacticity has been shown to have dramatic effects on the physical properties of polymers,[10,72] engineering stereo-microstructures of polymers to achieve desired target properties without changing the chemical composition should be a more sustainable strategy. In this context, through regulating tacticities (the range of isotactic [*mm*], syndiotactic [*rr*], and heterotactic [*mr*] distributions) by employing the ROP of a mixture of racemic (*R,S*)-*β*-BL and enantiopure (*R*)-*β*-BL in different ratios, Doi et al. showed that the mechanical properties of P3HB can be largely tuned from high T_m (177 °C) *it*-P3HB that is hard, rigid, and strong but brittle to low T_m (52, 62 °C) *sr*-P3HB [P_r (the probability of racemic linkages between two consecutive monomer units) = 0.70] that is soft (elastic modulus E = 20 MPa) and weak (σ_B = 13 MPa) but ductile.[73] Mehrkhodavandi et al.[64] reported that the ROP of *rac*-(*R,S*)-*β*-BL by a chiral zinc catalyst afforded melt-processable *sr*-P3HB (P_r = 0.64) that is strong, ductile, and tough, but its low T_m (46, 66 °C) would limit its application. In comparison, *at*-P3HB is a soft (E = 7 MPa), flexible (ε_B = 380%), and weak (σ_B = 6.5 MPa) elastomer.[64]

We reasoned that the ROP of *meso*-(*R,S*)-8DL^{Me} will inherently result in a *sr*-P3HB, even with an achiral, nonstereo-selective catalyst because repeating units will always produce an *r* diad, and therefore, the P_r will always be >0.5. Also unique to this system, the resulting *sr*-P3HB is inherently devoid of any [*mm*] triads (Figure 1). Thus, we hypothesized that a unique balance of stereo-regularity-dependent crystallinity and performance properties could be attained through the ROP of *meso*-8DL^{Me} by a nonstereo-selective catalyst, affording *sr*-P3HB with a controlled level of stereo-defects that can render a suitable level of crystallinity to overcome the above-overviewed trade-offs between crystallinity and ductility or processability. Indeed, *sr*-P3HB resulting from the ROP of *meso*-8DL^{Me} consists of 53% [*rr*], 47% [*mr*], and 0% [*mm*], giving a P_r of 0.77. This unique tacticity distribution brings about a synergistic combination of attractive properties, including crystallinity (T_m = 114 °C), optical transparency (due to very small spherulites), high elongation at break (ε_B >

https://doi.org/10.1021/jacs.2c12897
J. Am. Chem. Soc. 2023, 145, 5795−5802

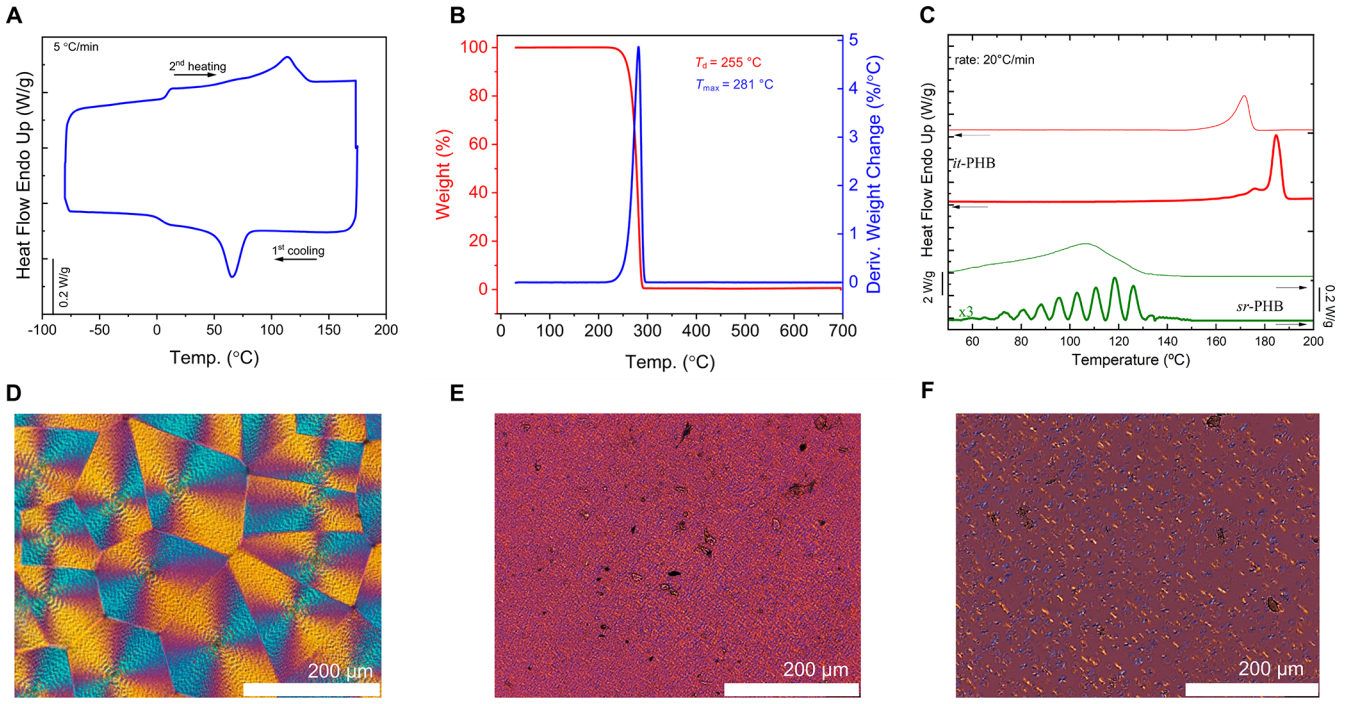

Figure 2. (A) Differential scanning calorimetry (DSC) curves of *sr*-P3HB (M_n = 171 kDa, $Đ$ = 1.07). (B) Thermogravimetric analysis (TGA) and derivative thermogravimetry (DTG) curves of *sr*-P3HB. (C) Thin lines: DSC second heating curves at 20 °C/min of *sr*-P3HB (green) and *it*-P3HB[78] (red); thick lines: final DSC heating scans after the SSA protocol for *sr*-P3HB (green) and *it*-P3HB (red). (D) PLOM micrographs for *it*-P3HB.[78] (E) PLOM micrographs for *sr*-P3HB. Micrographs were taken at 25 °C after melting for 1 min at 190 °C and cooling at 20 °C. (F) PLOM micrographs for *sr*-P3HB at 65 °C after holding for 1 min at 230 °C and cooling at 20 °C/min.

400%) and tensile strength (σ_B = 34 MPa), and excellent toughness (U_T = 96 MJ/m^3) while maintaining biodegradability in freshwater and soil.

RESULTS AND DISCUSSION

Synthesis of *sr*-P3HB by ROP of *meso*-8DL^{Me} with an Achiral Catalyst. The monomer employed in this study, *meso*-8DL^{Me}, is considered a (waste) coproduct in the *rac*-8DL^{Me} synthesis.[66,67] The ROP of *meso*-8DL^{Me} at room temperature (RT, ~25 °C) was investigated using the commercially available, achiral precatalyst La[N(SiMe$_3$)$_2$]$_3$, in combination with 3 equiv of an alcohol initiator. Among the three initiators examined, Ph$_2$CHOH outperformed PhCH$_2$OH, followed by the least effective Ph$_3$COH, attributable to the balanced acidity and sterics of Ph$_2$CHOH achieving both rapid alcoholysis of the precatalyst and preventing aggregation of the resulting alkoxy catalyst (Table 1, runs 1−3). Upon optimization, the ROP with a [*meso*-8DL^{Me}]/[La]/[Ph$_2$CHOH] ratio of 5000:1:3 (0.02 mol % catalyst) at RT achieved 89% monomer conversion in 22 min, affording high molar mass *sr*-P3HB with low dispersity (M_n = 171 kDa, $Đ$ = 1.07, Table 1, run 4).

Noteworthy is that the *sr*-P3HB produced here is inherently different from the *st*-P3HB obtained from *β*-BL as, in principle, it is not possible for the ROP of *meso*-8DL^{Me} to produce [*mm*] triads. The lack of [*mm*] triads is inherent to the coordination-insertion ROP mechanism of *meso*-8DL^{Me} as two opposite stereo-centers are always enchained together at each propagation step, making it impossible for three of the same stereo-centers added consecutively without invoking other side reactions such as transesterification (Figure 1B,C). The stereo-microstructure of *sr*-P3HB was confirmed by ^{13}C NMR analysis, showing no [*mm*] stereo-sequence but [*rr*] (53%) and [*mr*] (47%) and giving P_r = 0.77 (Figures 1D and S11). The potential epimerization of *meso*-8DL^{Me} (or racemization to *rac*-8DL^{Me}) during the ROP process can be ruled out on the basis of the NMR studies that showed that no [*mm*] triads are present in *sr*-P3HB (Figure S11) and that the crude polymerization mixture still containing residual (unreacted) *meso*-8DL^{Me} showed no formation of *rac*-8DL^{Me} (Figure S12).

Thermal Properties and Crystallization Behavior. The highly stereo-regular *it*-P3HB and *st*-P3HB have a high T_m of ~175 °C but a relatively low degradation temperature (T_d, defined as the temperature at 5% weight loss) of ~250 °C, which gives a narrow processing window and makes melt-processing challenging.[63,66] In comparison, *sr*-P3HB, designed as such herein, exhibits a lower T_m of 114 °C (heat of fusion, ΔH_f = 26.7 J/g), while the T_d is maintained at 255 °C (Figure 2A,B), thus giving *sr*-P3HB a much wider processing window. It is apparent that *sr*-P3HB shows a much broader melting transition than *it*-P3HB and *st*-P3HB with higher crystallinity.[61,67]

To better understand this difference, successive self-nucleation and annealing (SSA) thermal fractionation studies were performed on *sr*-P3HB and on *it*-P3HB for comparison purposes.[74,75,76,77] We found that *sr*-P3HB can be successfully fractionated by SSA, producing a number of clear and well-resolved thermal fractions (Figure 2C) with a monomodal distribution. In contrast, *it*-P3HB has a different SSA thermal fractionation profile: there is only one main thermal fraction and a minor secondary one, attesting to its highly regular isotactic structure (Figure 2C, red thick line curve). This behavior occurs because the thermal fractionation ability of any material increases as the number of defects that can interrupt the linear and stereo-regular crystallizable sequences increases. The tacticity defects present in *sr*-P3HB are randomly

https://doi.org/10.1021/jacs.2c12897
J. Am. Chem. Soc. 2023, 145, 5795−5802

distributed along the chain (hence their monomodal distribution of melting peaks after SSA fractionation[76,77]), and they frequently interrupt crystallizable sequences. This frequent interruption reduces its degree of crystallinity (73% for *it*-P3HB vs 15% for *sr*-P3HB after the SSA treatment) and its melting temperature. Figure 2D shows a polarized light optical microscopy (PLOM) image of *it*-P3HB,[78] and it is compared with a micrograph obtained for the *sr*-P3HB sample (Figure 2E) under the same cooling conditions from the melt (20 °C/min). The *it*-P3HB sample is characterized by large spherulites (>150 μm).[49,50] Instead, *sr*-P3HB has a morphology characterized by a submicron spherulitic texture, which will induce optical transparency as the characteristic crystalline aggregates are smaller than the typical wavelength of visible light (i.e., 400 nm) and will not produce any light scattering. This morphology is a consequence of the much higher nucleation density of *sr*-P3HB induced smaller than the typical wavelength of visible light (i.e., 400 nm) and will not produce any light scattering. This morphology is a consequence of the much higher nucleation density of *sr*-P3HB induced by the tacticity defects along the chains. To obtain a larger microspherulitic texture, a heat treatment was performed to *sr*-P3HB followed by isothermal crystallization at 65 °C (Figure 2F). Even so, the microspherulites obtained are still orders of magnitude smaller than those in *it*-P3HB.

Mechanical Properties. Tensile testing of *sr*-P3HB with M_n = 171 kDa ($Đ$ = 1.07) was performed on dog-bone specimens (ASTM D638 standard; type V) showing a high σ_B of 33.8 ± 1.4 MPa and an elastic modulus (E) of 217 ± 12 MPa (Figure 3). More impressively, this *sr*-P3HB material

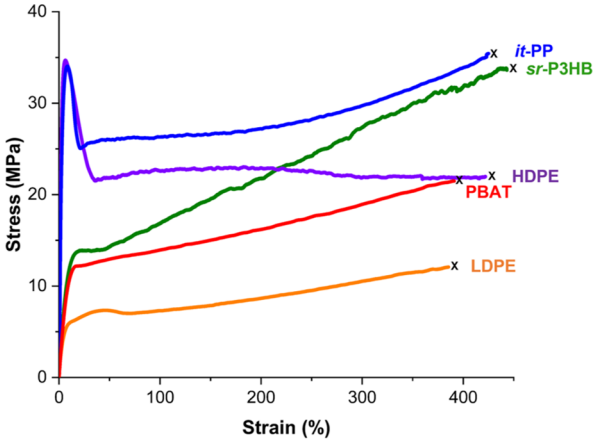

Figure 3. (A) Stress−strain curve overlays of *sr*-P3HB (green) with commercialized commodity plastics including *it*-PP (blue), HDPE (purple), PBAT (red), and LDPE (orange). Strain rate: 5.0 mm/min, ambient temperature.

exhibits an excellent ε_B of 419 ± 25% and overall high toughness (U_T) of 96 ± 6 MJ/m^3, making it over 100 times tougher than *it*-P3HB (σ_B = ∼35 MPa, ε_B ∼ 3−5%, U_T ∼ 0.6−0.9 MJ/m^3). This large difference in toughness is because *sr*-P3HB has a much lower degree of crystallinity and, at the same time, a refined microspherulitic texture that is expected to lead to higher ductility.

To ascertain the commercial relevance of *sr*-P3HB, the tensile properties were compared to high-density polyethylene (HDPE), low-density polyethylene (LDPE), polybutylene adipate terephthalate (PBAT), and isotactic polypropylene (*it*-PP) (Figure 3). Relative to the high-performance *it*-PP (M_n = 97 kDa), the *sr*-P3HB exhibits comparable σ_B and ε_B values. When compared to HDPE (melt flow index, MFI = 7.6) and LDPE (MFI = 7.5), the *sr*-P3HB shows a similar ε_B but a considerably higher σ_B. It also outperforms PBAT (M_n = 88.5 kDa, σ_B = 21.4 MPa, ε_B = 400%),[79] a commercialized biodegradable alternative to LDPE. These comparative studies demonstrate that the mechanical properties of *sr*-P3HB are competitive with both commodity plastics and their established biodegradable alternatives. Worth noting here is that the highly stereo-regular *st*-P3HB (P_r = 0.92, T_m = 169 °C, produced by stereo-selective ROP of *meso*-8DL^{Me} with a chiral catalyst, Table S1, Figures S5 and S6) is even too brittle to process into film specimens for tensile testing, behaving much like *it*-P3HB.

The best mechanical properties of any semicrystalline material are manifested between T_g and T_m. Toughness can only develop in this temperature range. As long as the use temperature is above T_g, the amorphous chains will be rubbery and flexible, allowing for ductility to develop depending on the degree of crystallinity and morphology of the material (i.e., spherulitic size). In this respect, *it*-PP also has a T_g around 0 °C, which limits its applications at temperatures below T_g because it will develop a brittle behavior. Even at room temperature, *it*-PP can be fragile (especially at high loading speeds, like during impact testing) if the thermal history (slow cooling) allows for the production of large spherulites and high crystallinity. This is why nucleating agents are usually added to *it*-PP to reduce the spherulitic size and produce a refined microspherulitic morphology affording transparency and toughness. Likewise, P3HB also has a T_g value of around 0 °C or slightly below zero, depending on its stereo-regularity and molar mass, and also develops large spherulites which concentrate stresses and provoke brittle fracture. In this work, the unique set of stereo-microstructures comprising enriched (53%) syndiotactic [*rr*], no isotactic [*mm*] triads but abundant (47%) stereo-defects ([*mr*]) randomly distributed along the polymer chain interrupts the perfectly regular crystallizable sequences, achieving two important effects: increasing nucleation density (hence producing a submicrospherulitic morphology leading to excellent transparency) and reducing crystallinity. Both effects, considering that room temperature is at least 25 °C above T_g, are crucial to significantly improve toughness.

Optical and Barrier Properties. The semicrystalline *sr*-P3HB was found to be optically clear by analysis of its transmittance and reflectance properties using an ultraviolet−visible near infraRed spectrophotometer, displaying a transmittance value (T %) of 92% and a reflectance value of 6.8% when scanned in the visible range (350 to 800 nm) (Figure S14). Compared to the transmittance values of commercial materials well-known for their excellent optical properties, *sr*-P3HB is as good as poly(methyl methacrylate) (PMMA; T % = 92%) and a 40-gallon Ziploc Bag (LDPE, T % = 89%), and far superior to *it*-P3HB (T % = 19%) (Figure 4). This high value of transmittance registered for *sr*-P3HB is due to its particular morphology constituted of very small superstructural aggregates (i.e., submicron spherulites, Figure 2E), unlike the low value of the *it*-P3HB transmittance, which is due to its much larger spherulites (Figure 2D).

The unusual synergistic coupling of excellent mechanical performance with optical transparency makes *sr*-P3HB attractive for packaging applications. In this context, the barrier properties of *sr*-P3HB were investigated and compared

https://doi.org/10.1021/jacs.2c12897
J. Am. Chem. Soc. 2023, 145, 5795−5802

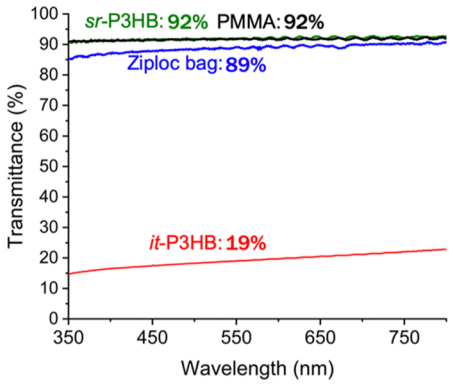

Figure 4. Transmittance overlays of *sr*-P3HB (green), PMMA (black), Ziploc Bag (blue), and *it*-P3HB (red).

to *it*-P3HB and several commodity plastics. Commercially available and biologically produced *it*-(*R*)-P3HB (Aldrich, M_w = 437 kDa) is known to have outstanding barrier properties with a low water vapor transmission rate (WVTR) of 0.5 ± 0.08 g mm m^{-2} day^{-1} and a low oxygen permeability (PO_2) of 0.01 ± 0.01 Barrer.[40] These barrier properties are attributed to the high degree of crystallinity of *it*-P3HB as the penetrants cannot be solubilized in the crystallites that create a tortuous pathway decreasing the diffusion coefficient and thus the permeability.[80] Because *sr*-P3HB has a lower degree of crystallinity compared to *it*-P3HB, it is expected that the barrier properties would be inferior. The PO_2 and *WVTR* for *sr*-P3HB (M_n = 110 kDa) were measured to be 0.15 ± 0.04 Barrer and 7.71 ± 0.68 g mm m^{-2} day^{-1} (Figure 5), respectively.

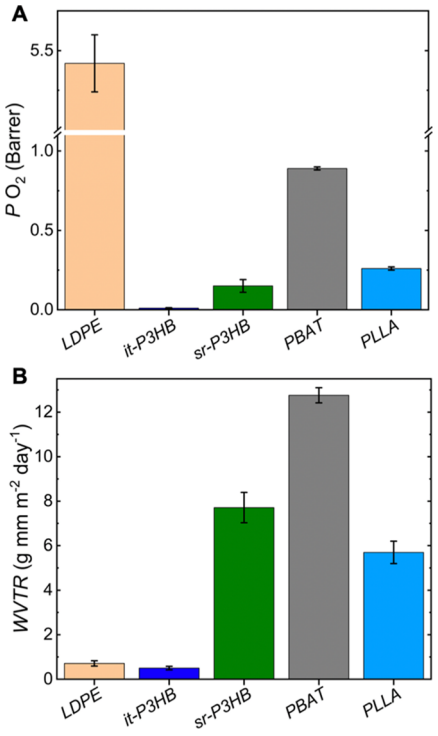

Figure 5. (A) Oxygen barriers of *sr*-P3HB compared to commercial plastics: 1 atm, 23 °C, 0% relative humidity. (B) Water vapor barriers of *sr*-P3HB compared to commercial plastics, 25 °C.

Nonetheless, the water vapor barrier of *sr*-P3HB is superior to that of PBAT and comparable with poly(L-lactic acid) (PLLA), while the oxygen barrier is far superior to LDPE, PBAT, and PLLA. Overall, *sr*-P3HB exhibits barrier properties that outcompete LDPE and commercialized biodegradable alternatives (PBAT and PLLA) in PO_2 and are comparable with PLLA and superior to PBAT in WVTR.

Biodegradability in Freshwater and Soil. The enzymatic degradation of P3HB with unnatural stereo-microstructures was investigated previously by Doi et al. using PHB depolymerase from *Pseudomonas pickettii*, and they reported that the rate of biodegradation depends on tacticity and that the *sr*-P3HB (P_r = 0.70) samples derived from the ROP of *β*-BL hardly degraded.[73] The biodegradability of the *sr*-P3HB produced by the ROP of *meso*-8DL^{Me} in this study was investigated in both freshwater and soil following the ISO 14851 and ASTM D5988-18 standards, respectively. Within 90 days, *sr*-P3HB reached ∼54% biodegradation under freshwater environment (25 °C), which is similar to that observed for the synthetic (*R*)-P3HB ([*mm*] > 0.99 produced by the enantioselective ROP of *rac*-8DL^{Me}) and the biologically produced (*R*)-P3HB (*bio*-P3HB) (Figure 6A). In soil environment, after 90 days *sr*-P3HB reached 50% biodegradation (Figure 6B). Through first-order kinetics, it can be predicted that *sr*-P3HB will reach 90% biodegradation in ∼268 days in soil and ∼383 days in freshwater (Table S3). For comparison, synthetic (*R*)-P3HB is estimated to reach 90% biodegradation in 145 days in soil and 433 days in freshwater. The *bio*-P3HB has a similarly estimated lifetime of 105 days in soil and 282 days in freshwater (Table S3).

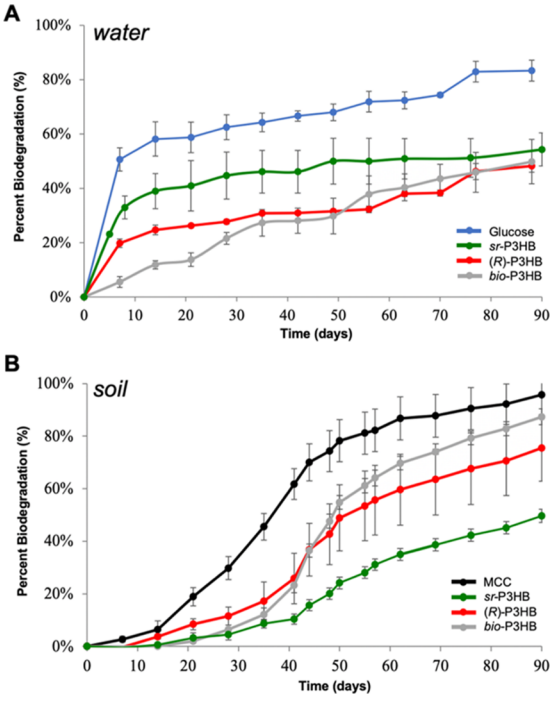

Figure 6. (A) Relative freshwater biodegradation results of *sr*-P3HB compared with synthetic (*R*)-P3HB, *bio*-P3HB, and glucose (control), 25 °C. (B) Relative soil biodegradation results of *sr*-P3HB compared with synthetic (*R*)-P3HB, *bio*-P3HB, and microcrystalline cellulose (control).

It is interesting to note that relative to *bio*-P3HB and synthetic (*R*)-P3HB, *sr*-P3HB displayed faster 90 day

https://doi.org/10.1021/jacs.2c12897
J. Am. Chem. Soc. 2023, 145, 5795−5802

biodegradation in freshwater (Figure 6A) but slower biodegradation in soil (Figure 6B). These differences may be attributed to the fact that freshwater and soil environments have different microbial populations and that the two testing environments differ modestly in temperature (freshwater at 25 °C vs soil at room temperature) and pH (freshwater at 7.2 vs soil at 7.4). Overall, these results suggest that if *sr*-P3HB is leaked into the soil or freshwater environment, it will efficiently biodegrade and leave no long-term accumulation in these environments.

CONCLUSIONS

In summary, we have synthesized *sr*-P3HB from the nonstereoselective ROP of *meso*-8DL^{Me}, the (waste) coproduct in the racemic diolide synthesis, using a simple, commercial, achiral catalyst. Thorough structure and property characterizations have revealed the unique set of stereo-microstructures of the current *sr*-P3HB, which are different from the previously disclosed *sr*-P3HB materials derived from the ROP of *β*-BL, and subsequently uncovered uniquely combined attractive properties, including crystallinity, optical transparency, toughness, commercially relevant barrier properties, and biodegradability. The stereo-microstructure of the *sr*-P3HB comprises enriched (53%) [*rr*] and no [*mm*] triads but abundant (47%) stereo-defects ([*mr* + *rm*]) randomly distributed along the chain. The origin of this unique set of stereo-microstructures for the *sr*-P3HB produced here is attributed to the *meso*-monomer structure, (*R*,*S*)-8DL^{Me} and the nonstereo-selectivity in the coordination-insertion ROP mechanism.

A particularly interesting and broader insight obtained from this work is that the randomly distributed, abundant stereo-defects along the *sr*-P3HB chain frequently interrupt crystallizable sequences and thus create a refined submicrospherulitic morphology that leads to the observed high optical transparency and ductility despite being semicrystalline with high tensile strength. In a nutshell, the stereo-defects present in *sr*-P3HB render its superior material properties in comparison to those of stereo-perfect or highly stereo-regular *it*-P3HB and *st*-P3HB. More broadly, these results further the more sustainable, monomaterial design approach that creates a diverse range of material properties of polymers via stereo-microstructural engineering without changing their chemical composition.

ASSOCIATED CONTENT

Supporting Information

The Supporting Information is available free of charge at https://pubs.acs.org/doi/10.1021/jacs.2c12897.

Experimental details, supporting figures and tables, and characterization data (PDF)

AUTHOR INFORMATION

Corresponding Authors

Alejandro J. Müller − *POLYMAT and Department of Polymers and Advanced Materials: Physics, Chemistry and Technology, Faculty of Chemistry, University of the Basque Country UPV/EHU, Donostia-San Sebastián 20018, Spain; IKERBASQUE, Basque Foundation for Science, Bilbao 48009, Spain;* orcid.org/0000-0001-7009-7715; Email: alejandrojesus.muller@ehu.es

Eugene Y.-X. Chen − *Department of Chemistry, Colorado State University, Fort Collins, Colorado 80523-1872, United States;* orcid.org/0000-0001-7512-3484; Email: eugene.chen@colostate.edu

Authors

Ethan C. Quinn − *Department of Chemistry, Colorado State University, Fort Collins, Colorado 80523-1872, United States;* orcid.org/0000-0002-9609-806X

Andrea H. Westlie − *Department of Chemistry, Colorado State University, Fort Collins, Colorado 80523-1872, United States*

Ainara Sangroniz − *Department of Chemistry, Colorado State University, Fort Collins, Colorado 80523-1872, United States; POLYMAT and Department of Polymers and Advanced Materials: Physics, Chemistry and Technology, Faculty of Chemistry, University of the Basque Country UPV/EHU, Donostia-San Sebastián 20018, Spain*

Maria Rosaria Caputo − *POLYMAT and Department of Polymers and Advanced Materials: Physics, Chemistry and Technology, Faculty of Chemistry, University of the Basque Country UPV/EHU, Donostia-San Sebastián 20018, Spain*

Shu Xu − *Argonne National Laboratory, Lemont, Illinois 60439, United States;* orcid.org/0000-0002-2713-7897

Zhen Zhang − *Department of Chemistry, Colorado State University, Fort Collins, Colorado 80523-1872, United States*

Meltem Urgun-Demirtas − *Argonne National Laboratory, Lemont, Illinois 60439, United States*

Complete contact information is available at: https://pubs.acs.org/10.1021/jacs.2c12897

Notes

The authors declare the following competing financial interest(s): A patent has been filed by Colorado State University Research Foundation on findings reported here.

ACKNOWLEDGMENTS

We gratefully acknowledge support by the U.S. Department of Energy, Office of Energy Efficiency and Renewable Energy, Advanced Manufacturing Office (AMO) and Bioenergy Technologies Office (BETO). This work was performed as part of the BOTTLE Consortium and funded under contract no. DE-AC36-08GO28308 with the National Renewable Energy Laboratory, operated by Alliance for Sustainable Energy. In the early stage of the PHA project, the work was supported by the U.S. National Science Foundation (NSF-1955482). A.J.M and M.R.C. acknowledge funding from the Basque Government through grant IT1503-22.

REFERENCES

(1) Sullivan, K. P.; Werner, A. Z.; Ramirez, K. J.; Ellis, L. D.; Bussard, J. R.; Black, B. A.; Brandner, D. G.; Bratti, F.; Buss, B. L.; Dong, X.; Haugen, S. J.; Ingraham, M. A.; Konev, M. O.; Michener, W. E.; Miscall, J.; Pardo, I.; Woodworth, S. P.; Guss, A. M.; Román-Leshkov, Y.; Stahl, S. S.; Beckham, G. T. Mixed Plastics Waste Valorization through Tandem Chemical Oxidation and Biological Funneling. *Science* **2022**, *378*, 207−211.

(2) Jehanno, C.; Alty, J. W.; Roosen, M.; De Meester, S.; Dove, A. P.; Chen, E. Y.-X.; Leibfarth, F. A.; Sardon, H. Critical Advances and Future Opportunities in Upcycling Commodity Polymers. *Nature* **2022**, *603*, 803−814.

(3) Law, K. L.; Narayan, R. Reducing Environmental Plastic Pollution by Designing Polymer Materials for Managed End-of-Life. *Nat. Rev. Mater.* **2022**, *7*, 104−116.

(4) Zhang, X.; Fevre, M.; Jones, G. O.; Waymouth, R. M. Catalysis as an Enabling Science for Sustainable Polymers. *Chem. Rev.* **2018**, *118*, 839−885.
(5) Hong, M.; Chen, E. Y.-X. Chemically Recyclable Polymers: A Circular Economy Approach to Sustainability. *Green Chem.* **2017**, *19*, 3692−3706.
(6) Schneiderman, D. K.; Hillmyer, M. A. 50th Anniversary Perspective: There Is a Great Future in Sustainable Polymers. *Macromolecules* **2017**, *50*, 3733−3749.
(7) Rahimi, A. R.; Garciá, J. M. Chemical Recycling of Waste Plastics for New Materials Production. *Nat. Rev. Chem.* **2017**, *1*, 0046.
(8) Garcia, J. M.; Robertson, M. L. The Future of Plastics Recycling. *Science* **2017**, *358*, 870−872.
(9) Shi, C.; Reilly, L. T.; Phani Kumar, V. S.; Coile, M. W.; Nicholson, S. R.; Broadbelt, L. J.; Beckham, G. T.; Chen, E. Y.-X. Design Principles for Intrinsically Circular Polymers with Tunable Properties. *Chem* **2021**, *7*, 2896−2912.
(10) Ellis, L. D.; Rorrer, N. A.; Sullivan, K. P.; Otto, M.; McGeehan, J. E.; Román-Leshkov, Y.; Wierckx, N.; Beckham, G. T. Chemical and Biological Catalysis for Plastics Recycling and Upcycling. *Nat. Catal.* **2021**, *4*, 539−556.
(11) Hou, Q.; Zhen, M.; Qian, H.; Nie, Y.; Bai, X.; Xia, T.; Laiq Ur Rehman, M.; Li, Q.; Ju, M. Upcycling and Catalytic Degradation of Plastic Wastes. *Cell Rep. Phys. Sci.* **2021**, *2*, 100514.
(12) Meys, R.; Kätelhön, M.; Bachmann, B.; Winter, C.; Zibunas, S.; Suh, S.; Bardow, A. Achieving net-zero greenhouse gas emission plastics by a circular carbon economy. *Science* **2021**, *374*, 71−76.
(13) Korley, L. T. J.; Epps, T. H.; Helms, B. A.; Ryan, A. J. Toward Polymer Upcycling-Adding Value and Tackling Circularity. *Science* **2021**, *373*, 66−69.
(14) Coates, G. W.; Getzler, Y. D. Y. L. Chemical Recycling to Monomer for an Ideal, Circular Polymer Economy. *Nat. Rev. Mater.* **2020**, *5*, 501−516.
(15) Teator, A. J.; Varner, T. P.; Knutson, P. C.; Sorensen, C. C.; Leibfarth, F. A. 100th Anniversary of Macromolecular Science Viewpoint: The Past, Present, and Future of Stereocontrolled Vinyl Polymerization. *ACS Macro Lett.* **2020**, *9*, 1638−1654.
(16) Tang, X.; Chen, E. Y.-X. Toward Infinitely Recyclable Plastics Derived from Renewable Cyclic Esters. *Chem* **2019**, *5*, 284−312.
(17) Nicholson, S. R.; Rorrer, N. A.; Carpenter, A. C.; Beckham, G. T. Manufacturing Energy and Greenhouse Gas Emissions Associated with Plastics Consumption. *Joule* **2021**, *5*, 673−686.
(18) Borrelle, S. B.; Ringma, J.; Law, K. L.; Monnahan, C. C.; Lebreton, L.; McGivern, A.; Murphy, E.; Jambeck, J.; Leonard, G. H.; Hilleary, M. A.; Eriksen, M.; Possingham, H. P.; De Frond, C. M.; Gerber, L. R.; Polidoro, B.; Tahir, A.; Bernard, M.; Mallos, N.; Barnes, M.; Rochman, C. M. Predicted Growth in Plastic Waste Exceeds Efforts to Mitigate Plastic Pollution. *Science* **2020**, *369*, 1515−1518.
(19) Nielsen, T. D.; Hasselbalch, J.; Holmberg, K.; Stripple, J. Politics and the Plastic Crisis: A Review throughout the Plastic Life Cycle. *Wiley Interdiscip. Rev.: Energy Environ.* **2020**, *9*, No. e360.
(20) *The New Plastics Economy - Rethinking the Future of Plastics* World Economic Forum, Ellen MacArthur Foundation, McKinsey & Company, 2016;
(21) Jambeck, J. R.; Geyer, R.; Wilcox, C.; Siegler, T. R.; Perryman, M.; Andrady, A.; Narayan, R.; Law, K. L. Plastic Waste Inputs from Land into the Ocean. *Science* **2015**, *347*, 768−771.
(22) Cywar, R. M.; Rorrer, N. A.; Hoyt, C. B.; Beckham, G. T.; Chen, E. Y.-X. Bio-Based Polymers with Performance-Advantaged Properties. *Nat. Rev. Mater.* **2022**, *7*, 83−103.
(23) Haider, T. P.; Völker, C.; Kramm, J.; Landfester, K.; Wurm, F. R. Plastics of the Future? The Impact of Biodegradable Polymers on the Environment and on Society. *Angew. Chem., Int. Ed.* **2019**, *58*, 50−62.
(24) Albertsson, A. C.; Hakkarainen, M. Designed to Degrade. *Science* **2017**, *358*, 872−873.
(25) Zhu, Y.; Romain, C.; Williams, C. K. Sustainable Polymers from Renewable Resources. *Nature* **2016**, *540*, 354−362.
(26) Sudesh, K.; Abe, H.; Doi, Y. Synthesis, Structure and Properties of Polyhydroxyalkanoates: Biological Polyesters. *Prog. Polym. Sci.* **2000**, *25*, 1503−1555.
(27) Bedade, D. K.; Edson, C. B.; Gross, R. A. Emergent Approaches to Efficient and Sustainable Polyhydroxyalkanoate Production. *Molecules* **2021**, *26*, 1−55.
(28) Tan, D.; Wang, Y.; Tong, Y.; Chen, G. Q. Grand Challenges for Industrializing Polyhydroxyalkanoates (PHAs). *Trends Biotechnol.* **2021**, *39*, 953−963.
(29) Anjum, A.; Zuber, M.; Zia, K. M.; Noreen, A.; Anjum, M. N.; Tabasum, S. Microbial Production of Polyhydroxyalkanoates (PHAs) and Its Copolymers: A Review of Recent Advancements. *Int. J. Biol. Macromol.* **2016**, *89*, 161−174.
(30) Muhammadi; Shabina; Afzal, M.; Hameed, S. Bacterial Polyhydroxyalkanoates-Eco-Friendly next Generation Plastic: Production, Biocompatibility, Biodegradation, Physical Properties and Applications. *Green Chem. Lett. Rev.* **2015**, *8*, 56−77.
(31) Laycock, B.; Halley, P.; Pratt, S.; Werker, A.; Lant, P. The Chemomechanical Properties of Microbial Polyhydroxyalkanoates. *Prog. Polym. Sci.* **2013**, *38*, 536−583.
(32) Chen, G. Q. A. Microbial Polyhydroxyalkanoates (PHA) Based Bio- and Materials Industry. *Chem. Soc. Rev.* **2009**, *38*, 2434−2446.
(33) Li, Z.; Yang, J.; Loh, X. J. Polyhydroxyalkanoates: Opening Doors for a Sustainable Future. *NPG Asia Mater.* **2016**, *8*, 1−20.
(34) Meereboer, K. W.; Misra, M.; Mohanty, A. K. Review of Recent Advances in the Biodegradability of Polyhydroxyalkanoate (PHA) Bioplastics and Their Composites. *Green Chem.* **2020**, *22*, 5519−5558.
(35) Taguchi, S.; Iwata, T.; Abe, H.; Doi, Y. *Poly(hydroxyalkanoate)s.*. In *Poly(hydroxyalkanoates)s in Polymer Science: A Comprehensive Reference*; Matyjaszewski, K., Möller, M., Eds.; Elsevier: Amsterdam, 2012, pp 157−182.
(36) Westlie, A. H.; Quinn, E. C.; Parker, C. R.; Chen, E. Y.-X. Synthetic Biodegradable Polyhydroxyalkanoates (PHAs): Recent Advances and Future Challenges. *Prog. Polym. Sci.* **2022**, *134*, 101608.
(37) Adamus, G.; Domiński, A.; Kowalczuk, M.; Kurcok, P.; Radecka, I. From Anionic Ring-Opening Polymerization of β-Butyrolactone to Biodegradable Poly(Hydroxyalkanoate)s: Our Contributions in This Field. *Polymers* **2021**, *13*, 4365.
(38) Li, H.; Shakaroun, R. M.; Guillaume, S. M.; Carpentier, J. F. Recent Advances in Metal-Mediated Stereoselective Ring-Opening Polymerization of Functional Cyclic Esters towards Well-Defined Poly(Hydroxy Acid)s: From Stereoselectivity to Sequence-Control. *Chem. - Eur. J.* **2020**, *26*, 128−138.
(39) Moore, T.; Adhikari, R.; Gunatillake, P. Chemosynthesis of Bioresorbable Poly(γ-Butyrolactone) by Ring-Opening Polymerisation: A Review. *Biomaterials* **2005**, *26*, 3771−3782.
(40) Sangroniz, A.; Zhu, J. B.; Tang, X.; Etxeberria, A.; Chen, E. Y.-X.; Sardon, H. Packaging Materials with Desired Mechanical and Barrier Properties and Full Chemical Recyclability. *Nat. Commun.* **2019**, *10*, 3559.
(41) Dove, A. P. Organic Catalysis for Ring-Opening Polymerization. *ACS Macro Lett.* **2012**, *1*, 1409−1412.
(42) Dunn, E. W.; Coates, G. W. Carbonylative Polymerization of Propylene Oxide: A Multicatalytic Approach to the Synthesis of Poly(3-Hydroxybutyrate). *J. Am. Chem. Soc.* **2010**, *132*, 11412−11413.
(43) Rieth, L. R.; Moore, D. R.; Lobkovsky, E. B.; Coates, G. W. Single-Site β-Diiminate Zinc Catalysts for the Ring-Opening Polymerization of β-Butyrolactone and β-Valerolactone to Poly(3-Hydroxyalkanoates). *J. Am. Chem. Soc.* **2002**, *124*, 15239−15248.
(44) Bruckmoser, J.; Henschel, D.; Vagin, S.; Rieger, B. Combining High Activity with Broad Monomer Scope: Indium Salan Catalysts in the Ring-Opening Polymerization of Various Cyclic Esters. *Catal. Sci. Technol.* **2022**, *12*, 3295−3302.
(45) Poirier, V.; Roisnel, T.; Carpentier, J. F.; Sarazin, Y. Versatile Catalytic Systems Based on Complexes of Zinc, Magnesium and Calcium Supported by a Bulky Bis(Morpholinomethyl)Phenoxy

https://doi.org/10.1021/jacs.2c12897
J. Am. Chem. Soc. 2023, 145, 5795−5802

Ligand for the Large-Scale Immortal Ring-Opening Polymerisation of Cyclic Esters. *Dalton Trans.* **2009**, 9820−9827.
(46) Kaminsky, W.; Funck, A.; Hähnsen, H. New Application for Metallocene Catalysts in Olefin Polymerization. *Dalton Trans.* **2009**, 8803−8810.
(47) Kamber, N. E.; Jeong, W.; Waymouth, R. M.; Pratt, R. C.; Lohmeijer, B. G. G.; Hedrick, J. L. Organocatalytic Ring-Opening Polymerization. *Chem. Rev.* **2007**, *107*, 5813−5840.
(48) Mahrova, T. V.; Fukin, G. K.; Cherkasov, A. V.; Trifonov, A. A.; Ajellal, N.; Carpentier, J. F. Yttrium Complexes Supported by Linked Bis(Amide) Ligand: Synthesis, Structure, and Catalytic Activity in the Ring-Opening Polymerization of Cyclic Esters. *Inorg. Chem.* **2009**, *48*, 4258−4266.
(49) Connor, E. F.; Nyce, G. W.; Myers, M.; Möck, A.; Hedrick, J. L. First Example of N-Heterocyclic Carbenes as Catalysts for Living Polymerization: Organocatalytic Ring-Opening Polymerization of Cyclic Esters. *J. Am. Chem. Soc.* **2002**, *124*, 914−915.
(50) Yang, J. C.; Yang, J.; Li, W. B.; Lu, X. B.; Liu, Y. Carbonylative Polymerization of Epoxides Mediated by Tri-Metallic Complexes: A Dual Catalysis Strategy for Synthesis of Biodegradable Polyhydroxyalkanoates. *Angew. Chem., Int. Ed.* **2022**, *61*e2021162.
(51) Tani, H.; Yamashita, S.; Teranishi, K. Stereospecific Polymerization of β-Methyl-β-Propiolactone. *Polym. J.* **1971**, *3*, 417−418.
(52) Agostini, D. D.; Lando, J.; Shelton, J. R. Synthesis and characterization of poly-β-hydroxybutyrate. I. Synthesis of crystalline DL-poly-β-hydroxybutyrate from DL-β-butyrolactone. *J. Polym. Sci. Part A Polym. Chem.* **1971**, *9*, 2775−2787.
(53) Teranishi, K.; Iida, M.; Araki, T.; Yamashita, S.; Tani, H. Stereospecific Polymerization of β-Alkyl-β-PropiolactoneStereospecific Polymerization of β-Alkyl-β-propiolactone. *Macromolecules* **1974**, *7*, 421−427.
(54) Bloembergen, S.; Holden, D. A.; Bluhm, T. L.; Hamer, G. K.; Marchessault, R. H. Stereoregularity in Synthetic β-Hydroxybutyrate and β-Hydroxyvalerate Homopolyesters. *Macromolecules* **1989**, *22*, 1656−1663.
(55) Inoue, S.; Tomoi, Y.; Tsuruta, T.; Furukawa, J. Organometallic-Catalyzed Polymerization of Propiolactone. *Makromol. Chem.* **1961**, *48*, 229−233.
(56) Zintl, M.; Molnar, F.; Urban, T.; Bernhart, V.; Preishuber-Pflügl, P.; Rieger, B. Variably Isotactic Poly(Hydroxybutyrate) from Racemic β-Butyrolactone: Microstructure Control by Achiral Chromium(III) Salophen Complexes. *Angew. Chem., Int. Ed.* **2008**, *47*, 3458−3460.
(57) Ajellal, N.; Durieux, G.; Delevoye, L.; Tricot, G.; Dujardin, C.; Thomas, C. M.; Gauvin, R. M. Polymerization of Racemic β-Butyrolactone Using Supported Catalysts: A Simple Access to Isotactic Polymers. *Chem. Commun.* **2010**, *46*, 1032−1034.
(58) Wu, B.; Lenz, R. W. Stereoregular Polymerization of [R,S]-3-Butyrolactone Catalyzed by Alumoxane-Monomer Adducts. *Macromolecules* **1998**, *31*, 3473−3477.
(59) Yang, R.; Xu, G.; Lv, C.; Dong, B.; Zhou, L.; Wang, Q. $Zn(HMDS)_2$ as a Versatile Transesterification Catalyst for Polyesters Synthesis and Degradation toward a Circular Materials Economy Approach. *ACS Sustainable Chem. Eng.* **2020**, *8*, 18347−18353.
(60) Bouyahyi, M.; Ajellal, N.; Kirillov, E.; Thomas, C. M.; Carpentier, J. F. Exploring Electronic versus Steric Effects in Stereoselective Ring-Opening Polymerization of Lactide and β-Butyrolactone with Amino-Alkoxy- Bis(Phenolate)-Yttrium Complexes. *Chem. - Eur. J.* **2011**, *17*, 1872−1883.
(61) Amgoune, A.; Thomas, C. M.; Ilinca, S.; Roisnel, T.; Carpentier, J. F. Highly Active, Productive, and Syndiospecific Yttrium Initiators for the Polymerization of Racemic β-Butyrolactone. *Angew. Chem., Int. Ed.* **2006**, *45*, 2782−2784.
(62) Zhuo, Z.; Zhang, C.; Luo, Y.; Wang, Y.; Yao, Y.; Yuan, D.; Cui, D. Stereo-Selectivity Switchable ROP of: Rac-β-Butyrolactone Initiated by Salan-Ligated Rare-Earth Metal Amide Complexes: The Key Role of the Substituents on Ligand Frameworks. *Chem. Commun.* **2018**, *54*, 11998−12001.
(63) Ajellal, N.; Bouyahyi, M.; Amgoune, A.; Thomas, C. M.; Bondon, A.; Pillin, I.; Grohens, Y.; Carpentier, J. F. Syndiotactic-Enriched Poly(3-Hydroxybutyrate)s via Stereoselective Ring-Opening Polymerization of Racemic β-Butyrolactone with Discrete Yttrium Catalysts. *Macromolecules* **2009**, *42*, 987−993.
(64) Kemnitzer, J. E.; McCarthy, S. P.; Gross, R. A. Syndiospecific Ring-Opening Polymerization of β-Butyrolactone To Form Predominantly Syndiotactic Poly(β-Hydroxybutyrate) Using Tin(IV) Catalysts. *Macromolecules* **1993**, *26*, 6143−6150.
(65) Ebrahimi, T.; Aluthge, D. C.; Hatzikiriakos, S. G.; Mehrkhodavandi, P. Highly Active Chiral Zinc Catalysts for Immortal Polymerization of β-Butyrolactone Form Melt Processable Syndio-Rich Poly(Hydroxybutyrate). *Macromolecules* **2016**, *49*, 8812−8824.
(66) Tang, X.; Chen, E. Y.-X. Chemical Synthesis of Perfectly Isotactic and High Melting Bacterial Poly(3-Hydroxybutyrate) from Bio-Sourced Racemic Cyclic Diolide. *Nat. Commun.* **2018**, *9*, 2345.
(67) Tang, X.; Westlie, A. H.; Watson, E. M.; Chen, E. Y.-X. Stereosequenced Crystalline Polyhydroxyalkanoates from Diastereomeric Monomer Mixtures. *Science* **2019**, *366*, 754−758.
(68) Zhang, Z.; Shi, C.; Scoti, M.; Tang, X.; Chen, E. Y.-X. Alternating Isotactic Polyhydroxyalkanoates via Site- and Stereoselective Polymerization of Unsymmetrical Diolides. *J. Am. Chem. Soc.* **2022**, *144*, 20016−20024.
(69) Tang, X.; Westlie, A. H.; Caporaso, L.; Cavallo, L.; Falivene, L.; Chen, E. Y.-X. Biodegradable Polyhydroxyalkanoates by Stereoselective Copolymerization of Racemic Diolides: Stereocontrol and Polyolefin-Like Properties. *Angew. Chem., Int. Ed.* **2020**, *59*, 7881−7890.
(70) Tang, X.; Shi, C.; Zhang, Z.; Chen, E. Y.-X. Toughening Biodegradable Isotactic Poly(3-Hydroxybutyrate) via Stereoselective Copolymerization of a Diolide and Lactones. *Macromolecules* **2021**, *54*, 9401−9409.
(71) Tang, X.; Shi, Z.; Zhang, E. Y.-X.; Chen, E. Y. X. Crystalline Aliphatic Polyesters from Eight-Membered Cyclic (Di) Esters. *J. Polym. Sci.* **2022**, *60*, 3478−3488.
(72) Worch, J. C.; Prydderch, H.; Jimaja, S.; Bexis, P.; Becker, M. L.; Dove, A. P. Stereochemical Enhancement of Polymer Properties. *Nat. Rev. Chem.* **2019**, *3*, 514−535.
(73) Abe, H.; Matsubara, I.; Doi, Y.; Hori, Y.; Yamaguchi, A. Physical Properties and Enzymic Degradability of Poly(3-Hydroxybutyrate) Stereoisomers with Different Stereoregularities. *Macromolecules* **1994**, *27*, 6018−6025.
(74) Müller, a J.; Hernández, Z. H.; Arnal, M. L.; Sánchez, J. J. A Novel Technique to Study Molecular Segregation during Crystallization. *Polym. Bull.* **1997**, *39*, 465−472.
(75) Arnal, M. L.; Balsamo, V.; Ronca, G.; Sánchez, A.; Müller, A. J.; Cañizales, E.; Urbina de Navarro, C. Applications of Successive Self-Nucleation and Annealing (SSA) to Polymer Characterization. *J. Therm. Anal. Calorim.* **2000**, *59*, 451−470.
(76) Müller, A. J.; Michell, R. M.; Pérez, R. A.; Lorenzo, A. T. Successive Self-Nucleation and Annealing (SSA): Correct Design of Thermal Protocol and Applications. *Eur. Polym. J.* **2015**, *65*, 132−154.
(77) Pérez-Camargo, R. A.; Cavallo, D.; Müller, A. J. Recent Applications of the Successive Self-Nucleation and Annealing Thermal Fractionation Technique. *Front. Soft Matter* **2022**, *2*, 1003500.
(78) Caputo, M. R.; Tang, X.; Westlie, A. H.; Sardon, H.; Chen, E. Y.-X.; Müller, A. J. Effect of Chain Stereoconfiguration on Poly (3-Hydroxybutyrate) Crystallization Kinetics. *Biomacromolecules* **2022**, *23*, 3847−3859.
(79) Sangroniz, A.; Sangroniz, L.; Aranburu, N.; Fernández, M.; Santamaria, A.; Iriarte, M.; Etxeberria, A. Blends of Biodegradable Poly(Butylene Adipate-Co-Terephthalate) with Poly(Hydroxi Amino Ether) for Packaging Applications: Miscibility, Rheology and Transport Properties. *Eur. Polym. J.* **2018**, *105*, 348−358.
(80) Yampolskii, Y.; Pinnau, I.; Freeman, B. D. *Materials Science of Membranes for Gas and Vapor Separation*; John Wiley and sons, Ltd: London, U.K., 2006.

https://doi.org/10.1021/jacs.2c12897
J. Am. Chem. Soc. 2023, 145, 5795−5802